Dual-wavelengths Filter Operating at Visible Wavelength Region using Subwavelength Grating on Waveguide Structure

Yuusuke Takashima[1], Masanobu Haraguchi[1], Yoshiki Naoi[1]

[1] Graduate School of Science and Technology, Tokushima University, 2-1 Minami-josanjima, Tokushima 770-8506, Japan

E-mail: takashima@ee.tokushima-u.ac.jp, Phone: +81 88 656 7447.

Abstract

A dual-wavelength filter was experimentally demonstrated using subwavelength grating (SWG)/waveguide structure. We designed the structural parameters of the SWG and the waveguide to find the reflection peaks in the visible wavelength region. To investigate the optical response of the designed SWG/waveguide structure, finite-difference time-domain (FDTD) numerical calculations were performed for electromagnetic field distribution. The dual reflection peaks from our proposed structure were predicted in visible wavelength regions by the FDTD calculation. The calculated electromagnetic field distribution also revealed that the reflection peaks were associated with resonances in the SWG and waveguides. We fabricated the SWG/waveguide with typical electron-beam lithography techniques, and two reflection peaks were observed at wavelengths of 486 nm and 590 nm with bandwidths of 45 nm and 58 nm, respectively. These experimental results indicate that dual-wavelength filters can be successfully realized without complex fabrication processes.

Keywords: Subwavelength grating, Waveguide, Dual-wavelength filter, Guided mode

1. Introduction

Recently, dual-wavelength filters have become one of the most important devices in many applications, such as high quality color filtering [1], imaging [2], and sensing [3]. For example, the temporal stability of a signal in the refractive index sensor has been improved using different optical fiber outputs between the two wavelengths because the background noise and intensity fluctuations of the light sources are cancelled out [4].

The most common dual-wavelength filter is based on the dye-polymer. Although the polymer-based filters have low cost, their operating wavelength region, the resistance for heat, and the bandwidth are influenced by the material characteristics of the polymers. This restricts the application fields of the wavelength filter. Tunable dual-wavelength filters operating in a visible region have been realized by the use of plasmonic metal nano-structure [5, 6]. The plasmonic wavelength filter transmits or reflects a certain two wavelengths and its operating wavelengths can be arbitrarily and easily controlled by adjusting the structural parameters. In spite of such wavelength tunability, the bandwidth of the transmitted or reflected light through the plasmonic structure is relatively broad, typically 100 nm, owing to the large light absorption in the metal.

Other groups theoretically proposed very narrow band dual-wavelength filters in infrared regions using guided mode in the asymmetric dielectric waveguides [7, 8]. Although the guided-mode-based filter achieved very narrow bandwidth, the cumbersome fabrication processes are still required, such as nano-grating pattering on the both sides of the thin dielectric film.

In this work, we experimentally and successfully achieved the dual-wavelength filter with subwavelength grating (SWG) and waveguide structure fabricated by a typical lithography process. Our filter is designed for the visible applications, such as refractive index sensing by using visible

fluorescent of proteins [9]. The broader bandwidth of the filter than that of fluorescent spectra deteriorates the spatial resolution of the fluorescent imaging. Also, too narrower filter bandwidth decreases the signal intensity of the fluorescence. Thus, we try to demonstrate the wavelength filter with similar bandwidth to that of typical fluorescent spectra of proteins (about 20-50nm) [10]. The finite-difference time-domain (FDTD) calculation was employed to investigate the optical response of our designed SWG/waveguide structure. The SWG/waveguide structure was also fabricated using the traditional monolithic lithography process and the two reflection peaks were experimentally obtained from the fabricated sample.

2. Design and fabrication of the dual-wavelength filter with SWG/waveguide

Here, we describe the design of the structural geometry of the SWG and waveguide for dual-wavelength filters operating in the visible region. The schematic of our filter is represented in Fig. 1.

The filter has two structural parts, one is the waveguide, and the other is the SWG. The waveguide structure is composed of the cladding, core, and substrate layers. The core layer, which has a high refractive index, is sandwiched between the low refractive index cladding layer and the substrate layer. The high refractive index SWG, whose period is shorter than the incident wavelength in free space, is on top of the waveguide. The grating period, grating stripe width, grating height, cladding layer thickness, and core layer thickness are represented by the symbols Λ, w, h, t_1, and t_2, respectively. The incident light normally enters the structure surface and propagates from the upper side of the SWG to the substrate region. The electric field of the incident light is shown as a red arrow in Fig. 1 and is perpendicular to the grating grooves.

For SWG, only the 0th order diffractions (namely transmission and reflection) occur, and

the higher diffraction orders are evanescent waves due to the shorter SWG period compared to the incident wavelength [11]. Inside the SWG, Bloch eigenmode sets are defined as the solutions of Maxwell's equations in periodic refractive index distribution [12]. The high refractive index contrast between the SWG and the ambient areas induces higher order eigenmodes in addition to the fundamental mode [13, 14]. These eigenmodes couple with the incident light when their wavenumbers coincide. Then, several excited eigenmodes travel in the SWG region and interfere with each other at the top and the bottom of the SWG [14, 15]. If destructive interference is formed at the bottom of the SWG, it will cancel the average fields between the air gap and grating bar, causing total internal reflection of the incident light. As a result, the resonance reflection peak is obtained [16-20].

In the waveguide structure, the guided modes, which are partially confined by the core layer, are excited by the evanescent higher order diffractions when the continuity of the wavenumber between these waves is satisfied [21]. The excited guided mode propagates along the core layer with total internal reflections at the SWG–core and core–substrate interfaces. At the SWG–core, internal reflections that are a part of the guided mode, are reradiated into the incident region by the SWG. If the reradiated waves from the waveguide constructively interfere with the 0th order reflected diffraction, the reflection peak appears in the reflection spectra of our structure [22-27]. Moreover, the core layer is separated from the ambient environment (herein, air) by cladding layer whereas the SWG is not. Thus, the ambient environment has different effects on the propagation characteristics of the SWG and waveguide modes. This is of great use in many applications of dual-wavelength filters, for example, refractive index sensing by dual wavelengths [4].

We designed the SWG/waveguide structures as dual-wavelength filters operating in the visible region using the wavenumber dispersion relationship of the eigenmode in the SWG and guided

mode in the waveguide [14, 21, 27]. Si_3N_4 was used for the SWG and the waveguide core material because it has a high refractive index value (about 2 in the visible region) and very low light absorption in the visible region [28]. SiO_2 and glass are used for the cladding and substrate of the waveguide owing to their low refractive index values and transparency [29]. To obtain dual reflection peaks in the visible wavelength region, the following structural parameters were chosen: Λ = 330 nm, w = 280 nm, h = 210 nm, t_1 = 40 nm, and t_2 = 210 nm.

The electromagnetic field distribution around the SWG/waveguide structure was calculated by a 2-dimensional FDTD method for investigation of the optical response of the structure. In the FDTD field calculation, the calculation region is divided into multiple spatial cells, and Maxwell's equations are directly solved in each cell. The model in the calculations is shown in Fig. 2. The calculation area was surrounded by dashed lines. The dashed lines represent the boundary conditions in this calculation. We employed periodic boundary condition (PBC) for x-directions and the electromagnetic field distribution in the calculation area infinitely repeats along the x-direction. We also assumed that the y-direction lengths of each structure components were infinite. These assumptions are justified, since the actual structure for y-direction is much larger than the incident wavelength. We employed a perfect matched layer (PML) as the z-direction boundary conditions to absorb the fields of the light outside the calculation area. The spatial cell size and the calculation interval time are 2×2 nm^2 and 4.7×10^{-18} s, respectively, and these values are enough to guarantee the convergence of the calculation. The p-polarized light, whose electric field oscillates for the x-direction, normally entered our designed SWG/waveguide structure. The reflected light intensity from the structure was calculated by Poynting vector through the observation monitor. The calculated reflection spectra are shown in Fig. 3 as a function of the incident wavelength. The reflection intensity was normalized by that of the incident

wave. In Fig. 3, the dual reflection peaks are observed at visible wavelengths of 505 nm and 555 nm. The full width at half maximum (FWHM) of these peaks are 50 nm and 20 nm, respectively. We also represent the electric field distribution inside the structure in order to interpret the origin of the reflection peaks.

The electric field distributions at each reflection peak are shown in Fig. 4. Figure 4 (a) and (b) show the x- and z-components of the electric field distribution at 505 nm. The field amplitudes were normalized by that of the incident field. The x-component electric fields in grating stripes and air gaps are in phase at the bottom of the SWG as shown in Fig. 4 (a), and the transmitted field is not cancelled. This distribution indicates that the destructive interference between the eigenmodes in the SWG does not occur. We also show z-components of the electric field distribution in Fig. 4 (b) to understand the physics of the reflection peak at 505 nm. We cannot generally observe the z-component of the field for the light propagating along z-direction because the light is a transverse wave, in which the electric and magnetic field are usually perpendicular to the propagation direction. However, the z-component electric field is observed at the SWG and core–substrate interfaces. The field distribution means that the evanescent diffraction of higher orders from the SWG couple with the guided mode propagating along the x-direction and the guided mode reflects at the core–substrate interface. These results indicate that the reflection peak at 505 nm results from the waveguide mode. We also show the x-component of the electric field distribution at 555 nm in Fig. 4 (c). The electric field distribution around the SWG is significantly distorted and the field amplitudes in grating bars and air gaps are opposite at the bottom of the SWG. As a result, the transmitted intensity is weakened and the incident light is almost reflected. This reveals that the destructive interference between eigenmodes inside SWG was formed [14] and the reflection peak at 555 nm is associated with the eigenmode interference

in SWG. The calculation results show that our designed structure can operate as a dual-wavelength filter.

3. Experimental results and discussion

Based on the theoretical consideration in the previous section, we fabricated the SWG and waveguide structure by using traditional electron beam lithography techniques. The fabrication process is as follows: we deposited 210 nm Si_3N_4 film onto the glass substrate. A SiO_2 film with the thickness of 40 nm was evaporated on the Si_3N_4 film. The Si_3N_4 film with a thickness of 210 nm was also deposited on the SiO_2 film. A thin film of EB resist (ZEP-520A: Zeon) was spin coated on the sample surface at 3000 rpm for 90 s. The thickness of the EB resist film was about 120 nm. We formed and developed the designed SWG pattern into the EB resistant film by using an EB lithography technique. A Ni metal mask with 50 nm thickness was evaporated onto the patterned resist film. The grating pattern was fabricated by inductive coupled plasma (ICP) etching. Finally, the metal mask was removed using diluted nitric acid. A scanning electron microscope image (SEM) of the surface of the fabricated SWG/waveguide is represented in Fig. 5. The SWG period and stripe width are 330 nm and 280 nm, respectively, and the SWG area is $300 \times 300\ \mu m^2$.

The reflection spectra of the fabricated sample were measured with the normal incident system. The light from a halogen source was p-polarized by a polarizer. The p-polarized light was focused and was normally entered to the sample surface using an objective lens (× 20 NA: 0.46). The reflected light intensity was measured by a spectrometer (Ocean Optics: USB 2000). The reflection spectra of the fabricated sample is shown in Fig. 6 as a function of the incident wavelength. The reflected intensity was normalized by that of the light source. The inset in Fig. 6 is the optical image of the sample. As shown in Fig. 6, the dual reflection peaks are experimentally observed at the visible wavelength of 486 nm (guided mode peak) and 590 nm (SWG peak), respectively. The experimental optical response of the fabricated sample shows good agreement with the theoretically predicted

sample. The FWHM of each peaks are 45 nm and 58 nm, respectively. The bandwidths of the experimental reflection peaks are narrower than those in metallic nano-structure-based wavelength filters [5, 6]. However, the experimental peak intensity at 590 nm is lower than that at 486 nm, and the bandwidth is about 3 times larger than calculated. The lower peak intensity and broader bandwidth at 590 nm can be attributed to the imperfect rectangle shape of the fabricated grating. The shape of SWG in the FDTD calculation is ideal while the fabricated SWG shape is not, owing to the ICP etching process (see Fig. 5). The imperfectness of the SWG shape induced the deviation of the eigenmode phase from that in the ideal rectangle SWG [30] and the deviation strongly influences the interference between the eigenmodes at the SWG bottom. Thus, the intensity and bandwidth of the experimental reflection peak resulting from the eigenmodes in SWG is different from what was theoretically calculated.

These experimental results indicate that we successfully demonstrated a dual-wavelength filter operating in a visible region. Moreover, we are able to monolithically fabricate the SWG/waveguide structure with a traditional lithography process and the ease of the fabrication is considerably useful for the various integration applications.

4 Conclusion

In conclusion, we attempted to produce a dual-wavelength filter via a typical lithography technique utilizing the SWG/waveguide structure. The wavenumber dispersion relation of the eigenmode in the SWG and waveguide is utilized for the design of the filter operating in the visible wavelength region. The FDTD calculated electromagnetic field distribution shows that dual sharp reflection peaks are expected in the designed structure and reveal the operation mechanism of our filter. We fabricated the SWG and waveguide structure on a glass substrate using a simple monolithic EB lithography process. The experimental reflection peaks are obtained at 486 nm and 590 nm with FWHMs of 45 nm and 58 nm, respectively; we thus experimentally and successfully demonstrated a dual-wavelength filter with a simple monolithic fabrication process. Our filter is suitable for integration devices owing to its ease of fabrication.

Acknowledgments

This work is partially supported by JSPS KAKENHI Grant Number JP18K04238 and the LED general platform project of Tokushima University.

References

[1] Mahani, F. F., Mokhtari, A., Mehran, M.: Dual mode operation, highly selective nanohole array-based plasmonic colour filters. Nanotechnology **28**, 385203 (2017).

[2] Xiao, L., Wei, L., Cheng, X., He, Y., Yeung, E. S.: Noise-free dual-wavelength difference imaging of plasmonic resonant nanoparticles in living cells. Anal. Chem. **83**, 7340-7347 (2011).

[3] Liu, D., Ngo, N. Q., Tjin, S. C., Dong, X.: A dual-wavelength fiber laser sensor system for measurement of temperature and strain. IEEE Photonics Technol. Lett. **19**, 1148-1150 (2007).

[4] Wang, S., Liu, S., Ni, W., Wu, S., Lu, P.: Dual-wavelength highly-sensitive refractive index sensor. Opt. Express **25**, 14389-14396 (2017).

[5] Li, Z., Clark, A. W., Cooper J. M.: Dual color plasmonic pixels create a polarization controlled nano color palette. ACS Nano **10**, 492-498 (2016).

[6] Kim, M., Kim, I., Jang, J., Lee, D., Nam, K. T., Rho, J.: Active color control in a metasurface by polarization rotation. Appl. Sci. **8**, 982 (2018).

[7] Liang, Y., Peng, W., Hu, R., Lu, M.: Symmetry-reduced double layer metallic grating structure for dual-wavelength spectral filtering. Opt. Express **22**, 11633-11645 (2014).

[8] Liang, Y., Peng, W., Lu, M., Chu, S.: Narrow-band wavelength tunable filter based on asymmetric double layer metallic grating. Opt. Express **23**, 14434-14445 (2015).

[9] van Manen, H.-J., Verkuijlen, P., Wittendorp, P., Subramaniam, V., van den Berg, T. K., Roos, D., Otto, C.: Refractive index sensing of green fluorescent proteins in living cells using fluorescence lifetime imaging microscopy. Biophys. J. **94**, L67-L69 (2008).

[10] Adams, K. E., Ke, S., Kwon, S., Liang, F., Fan, Z., Lu, Y., Hirschi, K., Mawad, M. E., Barry, M. A., Sevick-Muraca, E. M.: Comparison of visible and near-infrared wavelength-excitable fluorescent dyes for molecular imaging of cancer. J. Biomed. Opt. **12**, 024017 (2007).

[11] Kikuta, H., Toyota, H., Yu, W.: Optical elements with subwavelength structured surfaces. Opt. Rev. **10**, 63-73 (2003).

[12] Lalanne, P., Hugonin, J. P., Chavel P.: Optical properties of deep lamellar gratings: A coupled Bloch-mode insight. J. Lightwave Technol. **24**, 2442-2449 (2006).

[13] Chang-Hasnain C. J.: High-contrast gratings as a new platform for integrated optoelectronics. Semicond. Sci. Technol. **26**, 014043 (2011).

[14] Chang-Hasnain C. J., Yang, W.: High-contrast gratings for integrated optoelectronics. Adv. Opt. Photonics **4**, 379-440 (2012).

[15] Karagodsky, V., Sedgwick, F. G., Chang-Hasnain C. J.: Theoretical analysis of subwavelength high contrast grating reflectors. Opt. Express **18**, 16973-16988 (2010).

[16] Zhuang, L., Schablitsky, S., Shi, R. C., Chou, S. Y.: Fabrication and performance of thin amorphous Si subwavelength transmission grating for controlling vertical cavity surface emitting laser polarization. J. Vac. Sci. Technol. B **14**, 4055-4057 (1996).

[17] Zhou, Y., Moewe, M., Kern, J., Huang, M. C. Y., Chang-Hasnain, C. J.: Surface-normal emission of a high-Q resonator using a subwavelength high-contrast grating. Opt. Express **16**, 17282-17287 (2008).

[18] Gębski, M., Dems, M., Szerling, A., Motyka, M., Marona, L., Kruszka, R., Urbańczyk, D., Walczakowski, M., Palka, N., Wójcik-Jedlińska, A., Wang, Q. J., Zhang, D. H., Bugajski, M., Wasiak, M., Czyszanowski, T.: Monolithic high-index contrast grating: a material independent high-reflectance VCSEL mirror. Opt. Express **23**, 11674-11686 (2015).

[19] Hogan, B., Hegarty, S. P., Lewis, L., Romero-Vivas, J., Ochalsky, T. J., Huyet, G.: Realization of high-contrast gratings operating at 10 μm. Opt. Lett. **41**, 5130-5133 (2016).

[20] Takashima, Y., Haraguchi, M., Naoi, Y.: Highly sensitive magnetic field sensor with normal-incidence geometry using Ni-based bilayer subwavelength periodic structure operating in visible-wavelength region. Jpn. J. Appl. Phys. **57**, 08PE01 (2018).

[21] Park, C. H., Yoon, Y. T., Lee, S. S.: Polarization-independent visible wavelength filter incorporating a symmetric metal-dielectric resonant structure. Opt. Express **20**, 23769-23777 (2012).

[22] Liu, Z. S., Tibuleac S., Shin, D., Young, P. P., Magnusson R.: High-efficiency guided-mode resonance filter. Opt. Lett. **23**, 1556-1558 (1998).

[23] Wang, Z., Sang, T., Wang, L., Zhu, J., Wu, Y., Chen, L.: Guided-mode resonance Brewster filters with multiple channels. Appl. Phys. Lett. **88**, 251115 (2006).

[24] Yoon, Y. T., Park, C. H., Lee, S. S.: Highly efficient color filter incorporating a thin metal-dielectric resonant structure. Appl. Phys. Express **5**, 022501 (2012).

[25] Lee, K. J., Giese, J., Ajayi, L., Magnusson, R., Johnson, E.: Resonant grating polarizers made with silicon nitride, titanium dioxide, and silicon: Design, fabrication, and characterization. Opt. Express **22**, 9271-9281 (2014).

[26] He, S., Shi, Z., Li, X., Gao, X., Wang, Z., Liu, Q., Zhu, G., Zhang, M., Zhu, H., Wang, Y.: Membrane guided-mode resonant color filters exhibiting adjustable spectral response. Opt. Commun. **342**, 129-135 (2015).

[27] Sahoo, P. K., Sarker, S., Joseph, J.: High sensitivity guided-mode-resonance optical sensor employing phase detection. Sci. Rep. **7**, 7607 (2017).

[28] Luke, K., Okawachi, Y., Lamont, M. R. E., Gaeta, A. L., Lipson, M.: Broadband mid-infrared frequency comb generation in a Si_3N_4 microresonator. Opt. Lett. **40**, 4823-4826 (2015).

[29] Rodríguez-de Marcos, L. V., Larruquert, J. I., Méndez, J. A., Aznárez, J. A.: Self-consistent optical constants of SiO_2 and Ta_2O_5 films. Opt. Mater. Express **6**, 3622-3637 (2016).

[30] Sridharan, G., Bhattacharya, S.: Simplified analysis of sub-wavelength triangular gratings by simplified modal method. Appl. Opt. **55**, 9712-9718 (2016).

Figures captions

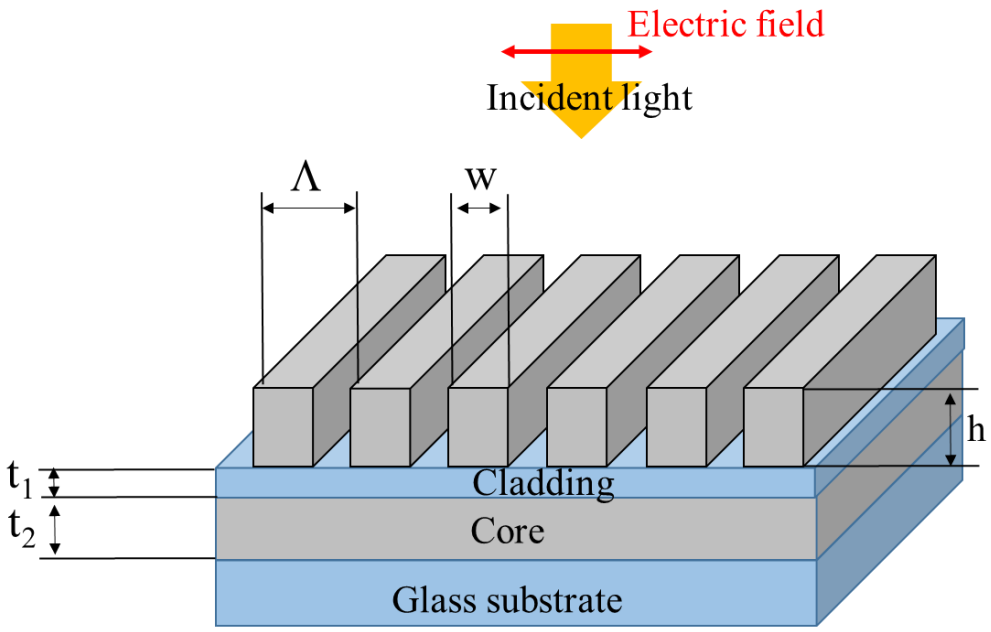

Fig. 1 Configuration of the dual-wavelength filter with SWG/waveguide. The waveguide is composed of substrate, core, and cladding layers. The SWG is placed on top of the waveguide. The grating period, grating stripe width, grating height, cladding layer thickness, and core layer thickness are represented by the symbols Λ, w, h, t_1, and t_2, respectively.

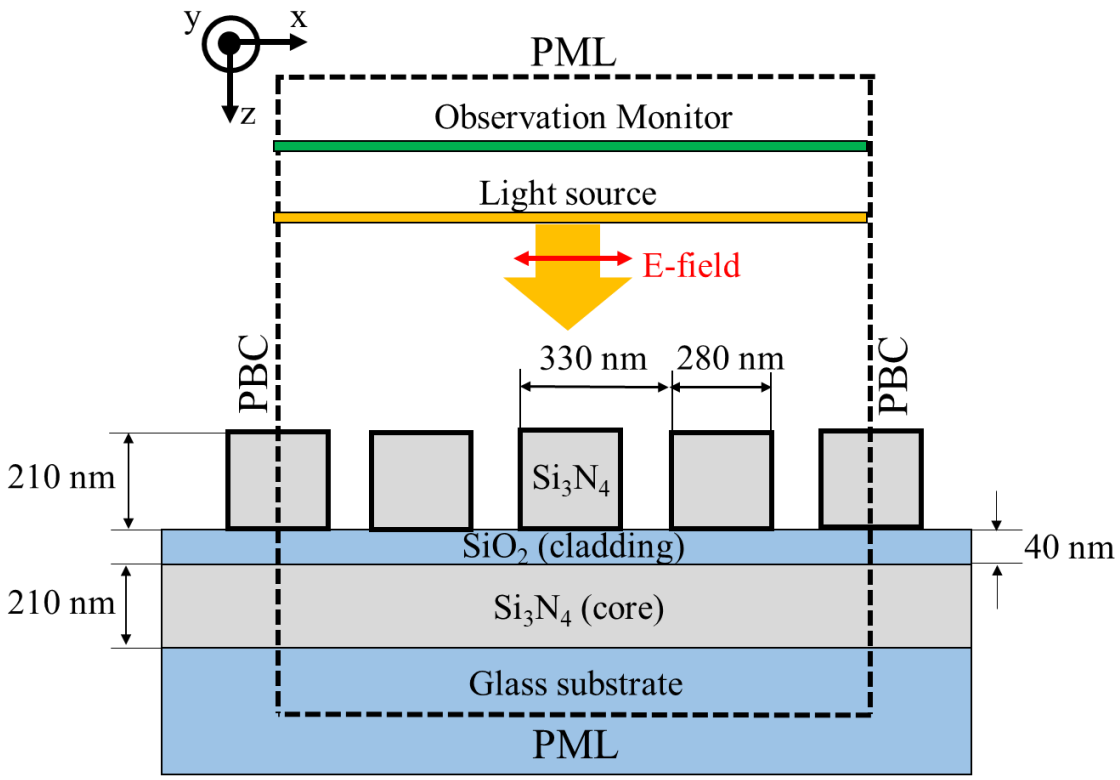

Fig. 2 Cross-sectional view of the FDTD calculation model. The dashed lines represent the boundary conditions. The p-polarized light, whose electric field oscillates in the x-direction, is propagated along the z-direction and normally entered our SWG/waveguide filter.

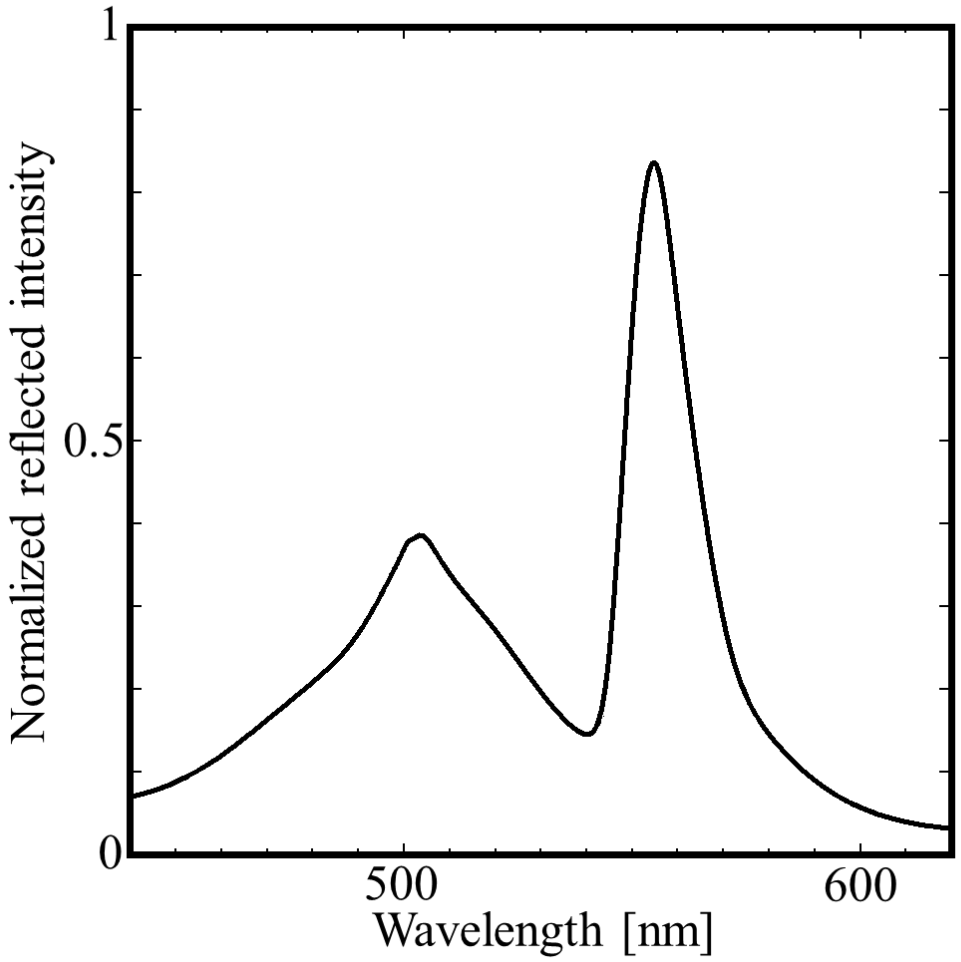

Fig. 3 Reflection spectrum of the SWG/waveguide structure by FDTD numerical calculation. The reflected light intensity was evaluated by the Poynting vector and was normalized by that of the incident light. The dual reflection peaks appeared at wavelengths of 505 nm and 555 nm.

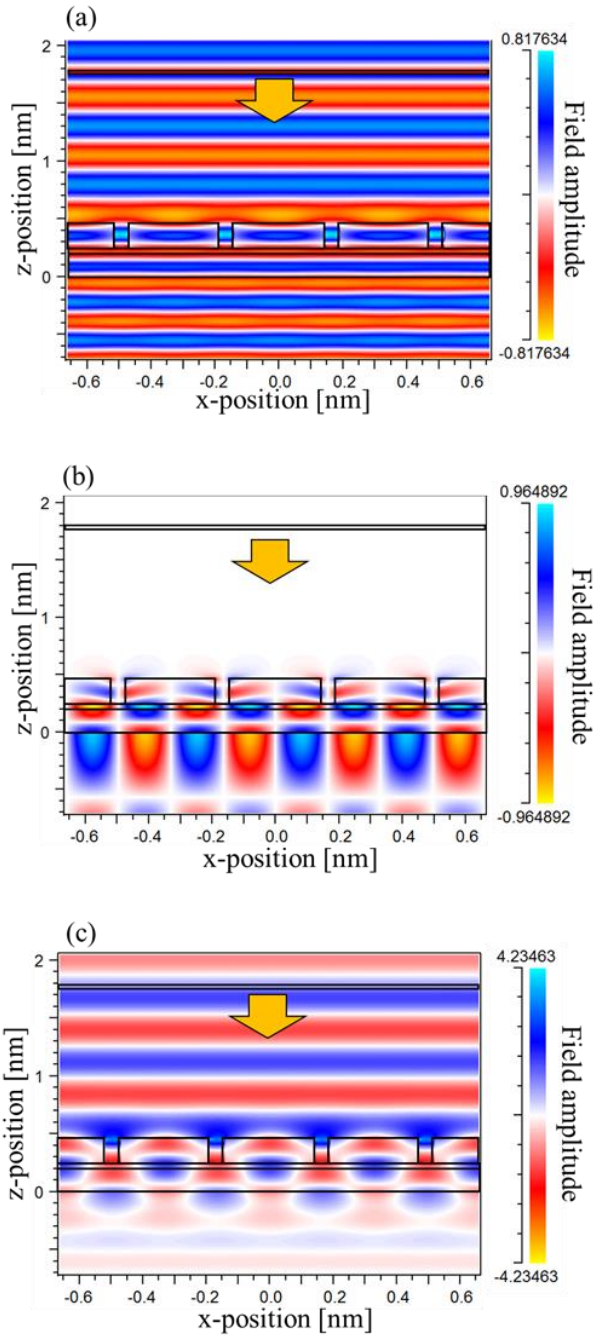

Fig. 4 Electric field distribution of SWG/waveguide at each reflection peak: (a) and (b) show the x- and z-components of the electric field distributions at 505 nm, and (c) shows the x-component of the electric field distribution at 555 nm. The field amplitudes of the distributions were normalized by that of the incident field.

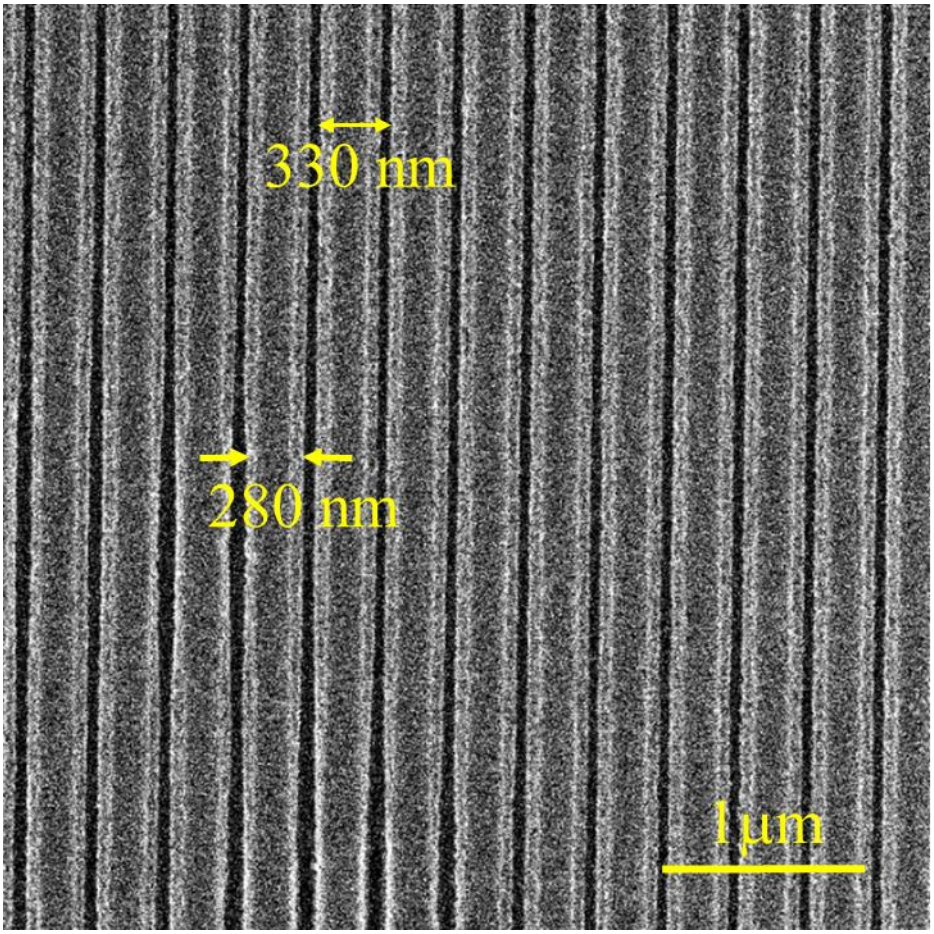

Fig. 5 SEM top view of the fabricated SWG/waveguide. The yellow line indicates a 1-μm scale bar. The period and the grating stripe width are 330 nm and 280 nm, respectively.

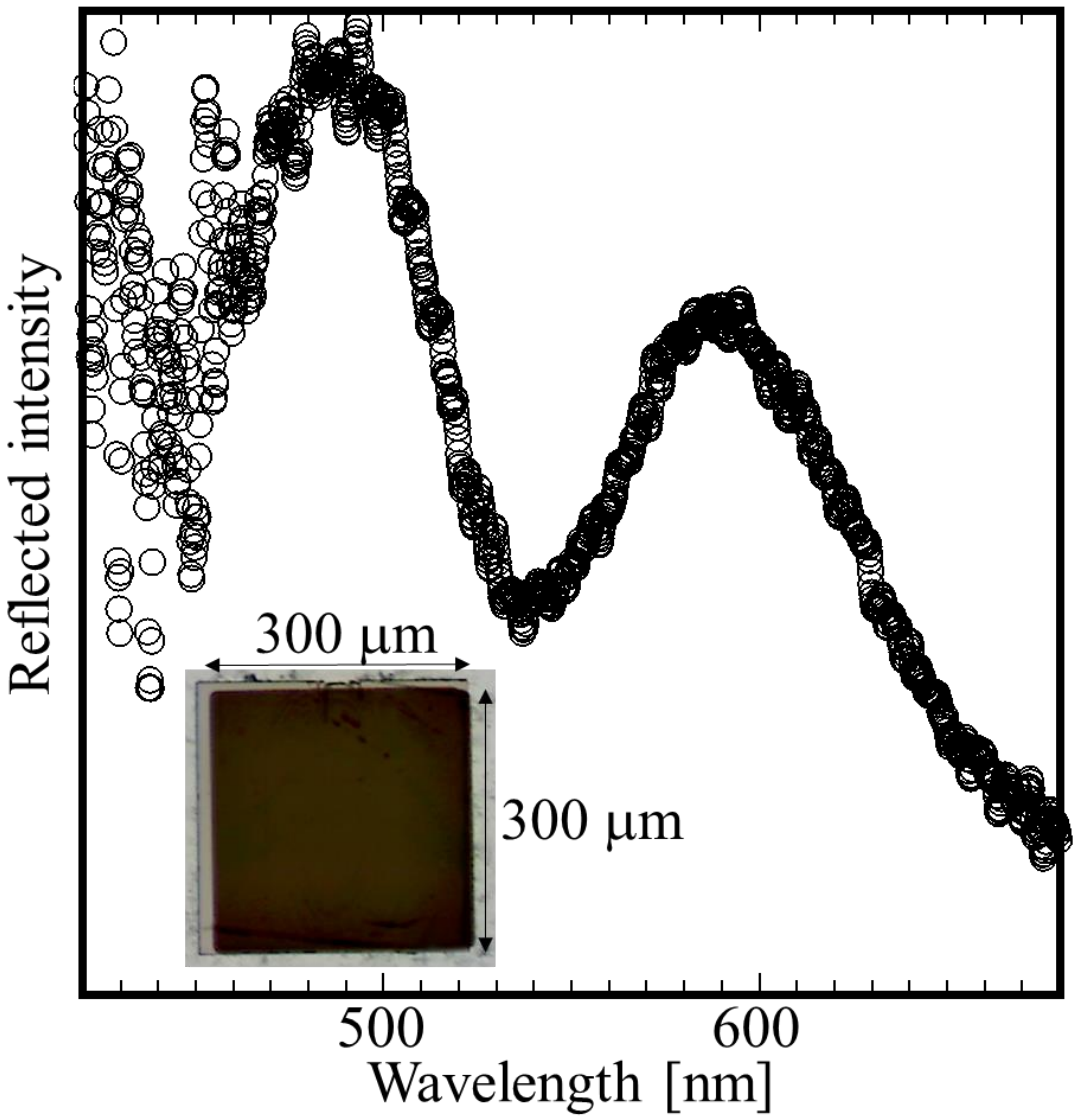

Fig. 6 Reflection spectrum of the fabricated sample as a function of the incident wavelength. The reflected intensity was normalized with that of the light source. The inset in Fig. 6 is the optical image of the sample. The dual reflection peaks are experimentally observed at the visible wavelengths of 486 nm and 590 nm.